Digital Autopilot for Thrust Vector Control of the Shuttle Orbital Maneuvering System

A. Penchuk* and S. Croopnick†
The Charles Stark Draper Laboratory, Inc., Cambridge, Massachusetts

This paper describes the requirements for and the design, development, and performance of the digital autopilots for thrust vector control, utilizing the orbital maneuvering system of the Space Shuttle Orbiter. The hardware and software requirements that led the design to its current form are described. Also, the design synthesis, which considered rigid-body stability margins, bending and slosh stabilization, guidance-loop compensation, off-nominal performance, and hardware and software limitations is presented. The performance of the orbital maneuvering system control system is summarized using flight data from the first three Space Transportation System flights.

Introduction

THE two orbital maneuvering system engines, which each produce 6000 lb thrust, provide a total orbital maneuvering system velocity change capability of approximately 1000 ft/s used for orbit insertion, circularization, orbital operations, and deorbit burns. The Orbiter is maneuvered in roll, pitch, and yaw during thrusting by controlling the gimbal angle of the orbital maneuvering system engines. The orbital maneuvering system processor is driven by a three-axis rate command from the steering processor coordinatized in the vehicle axes. The rate command is generated by processing either manual commands or automatic commands from the Orbiter's guidance system. During a two-engine burn, the orbital maneuvering system processor has the primary control responsibility for roll, pitch, and yaw, while the reaction control system is operated in parallel with wide deadbands in a backup or wraparound mode, exercising control only if the orbital maneuvering system control authority is inadequate. During a one-engine burn, the orbital maneuvering system processor controls pitch and yaw and the reaction control system processor has responsibility for roll.

The orbital maneuvering system may be considered to consist of the following four elements described herein: the measurements, the plant or vehicle to be controlled, the actuators, and the controller that contains the control laws. The design of the orbital maneuvering system thrust vector control system, as used in both the transition and on-orbit phases of the Shuttle flight, is the same except for the difference in the derivation of body angular rates. In the transiton phase, rates are obtained directly from the body-mounted rate gyro package. In the on-orbit digital autopilot they are derived by back differencing the inertial measurement unit attitude indications. This paper describes only the version used in the transition digital autopilot. The orbiter, for orbital maneuvering system thrust vector control system design purposes, is modeled as a rigid body with bending and propellant slosh effects superimposed on it. Despite the apparent sturdiness of the vehicle and the relatively small amount of orbital maneuvering system propellant, both of these effects may be significant and need to be considered in the design.

The orbital maneuvering system control effectors consist of two gimballed rocket engines, which are not throttleable, located as shown in Fig. 1. The electromechanical actuators that drive the engine gimbals are highly nonlinear servo systems and place constraints on the thrust vector control design due to their performance limitations in terms of deflection limits and cycle life. These constraints are quantified in the requirements section.

The controller, which is contained in the flight control module as shown in Fig. 2, is further divided into two parts: the thrust vector control law, which controls the inner loop, and steering, which controls the outer loop in the automatic mode. In the manual mode of thrust vector control, this steering function is performed using the rotational hand controller. The input to the thrust vector control law is the angular rate error, i.e., the difference between commanded and actual rates, and the controller output is the engine deflection command. The inputs to steering are the thrust direction vector from guidance and the velocity increments measured by the inertial measurement unit, and the output is the rate command to the inner loop. Most of the discussion in this paper concerns operation in the automatic mode in the absence of the reaction control system wraparound.

Requirements

The requirements for the orbital maneuvering sytem (OMS) thrust vector control (TVC) can be grouped in five categories: basic operation, response and stability, performance, failure tolerance, and TVC actuator constraints.

Basic Operation

OMS TVC in the pitch and yaw axes is implemented by pitch and yaw gimbal actuators for each OMS engine, with reaction control system (RCS) wraparound. Roll TVC is implemented by differential pitch gimballing with RCS wraparound if two OMS engines are thrusting, or by RCS alone if one OMS engine is thrusting.

In the manual mode, pitch and yaw rate commands are proportional to rotational hand-controller deflection, and the roll rate command is either likewise proportional with two OMS engines thrusting or three-level ($-\omega_c$, 0, $+\omega_c$) with one OMS engine thrusting. An RCS acceleration mode (a manual-command extension of the wraparound) is available in each axis when the hand controller is moved to a corresponding

Presented as Paper 82-1579 at the AIAA Guidance and Control Atmospheric Flight Mechanics and Astrodynamics Conference, San Diego, Calif., Aug. 9-11, 1982; submitted Aug. 27, 1982; revision received June 7, 1983.

*Staff Engineer. Member AIAA. Editor's Note: We regret to report that Mr. Penchuk died on Feb. 22, 1983.

†Section Chief. Member AIAA.

limit position. The automatic mode implements thrust-direction commands generated by the guidance system, using cross-product steering. In this mode only pitch and yaw rates are commanded; roll rate is held at zero.

Response and Stability of the Inner Loop

There are two response requirements: vehicle angular rate response to a step rate command input, and OMS gimbal angle response to a step torque disturbance (e.g., thrust misalignment or external torque). The expected responses are specified as time-domain envelopes and are identical for pitch and yaw. Table 1 gives the important parameters of the time envelopes assuming a two-engine burn. Percentages given in the table refer to the steady-state output change.

Stability margin requirements are specified in terms of gain and phase margins with the minimum value of gain margin set at 8 dB both below and above the crossover frequency, and the phase margin at 30 deg. These margins apply for transport lags up to 40 ms.

Performance

This is specified as a set of maximum permitted peak and residual cross-axis velocity errors assuming a two-engine burn, initial pitch and yaw attitude errors of 20 and 10 deg, respectively, a 2 deg/s/axis maximum commanded rate, and the following inputs to the cross-product steering law:

$$\bar{V}_{go} = \bar{V}_{\text{init}} - \bar{V}_t \qquad \Delta\bar{V} = \bar{V}_t - \bar{V}_{t-0.96}$$

where $\bar{V}_{go}$ is the commanded thrust direction, $\bar{V}_{\text{init}}$ the initial commanded velocity change, $\bar{V}_t$ the sensed vehicle velocity change over burn, at time t, and $\Delta\bar{V}_t$ the change in vehicle velocity in 0.96 s. Maximum velocity errors for these conditions are given in Table 2.

Failure Tolerance

The flight control system including OMS TVC and RCS wraparound must maintain attitude control during nominal two- and one-engine burns and also in the event of a single OMS engine failure. It also must act in opposition to a transient caused by OMS or RCS failure, although the response, stability, and performance critria cited earlier do not apply during such a transient. The crew is notified of OMS hardware failures and can optionally deselect one or both OMS engines or activate a standby actuator channel.

The crew also has procedures for shutting down a failed-on RCS jet, and a failed-off jet may be deselected automatically or by the crew. The transient is considered to end when the required reconfiguration (including activation of any redundant hardware) has occurred and operational or safe status is regained.

Table 1 Required response charactreistics

Step input	Maximum rise time, s (to %)	Maximum settling time, s (to %)	Maximum overshoot, %
0.5 deg/s rate command	6 (to 85)	20 (to ±15)	30
≤1 deg thrust misalignment or equivalent	10 (to 90)	20 (to ±10)	25

Table 2 TVC closed loop maximum velocity errors[a]

Burn duration s	Peak velocity error, ft/s Y	Peak velocity error, ft/s Z	Velocity residual, ft/s Y	Velocity residual, ft/s Z
200	5	10	0.25	0.25
100	5	10	0.5	0.5
50	5	10	1	1
25	5	10	5	8

[a]These errors are specified in an inertial frame of reference where the X axis is along $\bar{V}_{\text{init}}$, the Y axis is perpendicular to $\bar{V}_{\text{init}}$ and to the vehicle Z axis; the Z axis completes the triad.

TVC Actuator Constraints

Additional requirements are imposed on the OMS TVC due to actuator hardware constraints. The actuator activity average must be less than 1 cycle per second, where a cycle is defined as two on-off-on pulses. The other constraint limits the available range of commanded actuator deflections to ±5.89 deg for pitch and ±6.44 deg for yaw.

Design

The OMS TVC control system may be divided in two parts for analysis and discussion purposes. The function of one section of the control system called the "inner loop" is to achieve a commanded angular body rate. This commanded angular rate is generated by a steering section either manually or automatically. The overall vehicle response to a commanded thrust direction, which is the input to the steering section, is considered to be that of the "outer loop." It is comprised of both the steering and the inner-loop functions.

The portion of the control system that is implemented in the onboard digital computer is depicted in Fig. 3. The OMS processor is in the inner loop, whereas the steering processor is in the outer loop. The discussion is limited to the pitch channel, but is applicable to the yaw channel as well. The RCS processor is not shown since it does not affect the nominal pitch response.

Inner Loop

A block diagram of the OMS TVC inner loop is shown in Fig. 4. The plant is modeled as a rigid body with bending and slosh dynamics. The OMS engine servo is an electromechanical control system and modeled as consisting of an on-off amplifier, electric motor, gears, dynamic braking, mount compliance, engine inertia, and accompanying

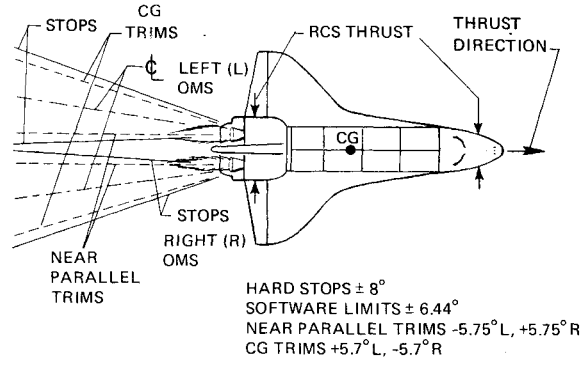

Fig. 1a Orbiter OMS yaw gimbal geometry.

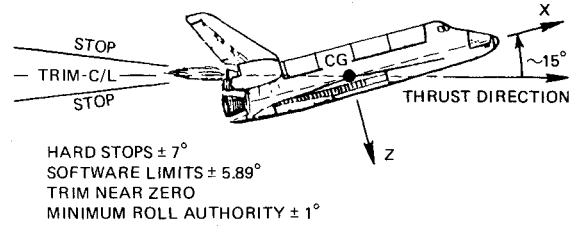

Fig. 1b Orbiter OMS pitch gimbal geometry.

nonlinearities such as friction and backlash. This whole system was adequately represented for analysis and simulation purposes by the simplified actuator model as shown in the figure. The main nonlinearity is the on-off amplifier with a deadband of 0.08 deg and hysteresis at 0.41 deg. K, the rate of travel of the engine, is nominally 4 deg/s and the limiter represents the hard stop of the actuator. The closed-loop gain and phase characteristics of the actuator loop were obtained experimentally[1] on a real actuator using the describing function technique. These characteristics were plotted as a function of frequency with the sinusoidal amplitude of the signal applied to the nonlinear system as a parameter. The plots were then approximated by transfer functions in order to facilitate the sampled data system analyses performed in the z and w planes.

The TVC law is the digital compensation part of the inner-loop synthesized in the w plane. It consists of a steady-state gain, a third-order low-pass filter, and integral compensation.

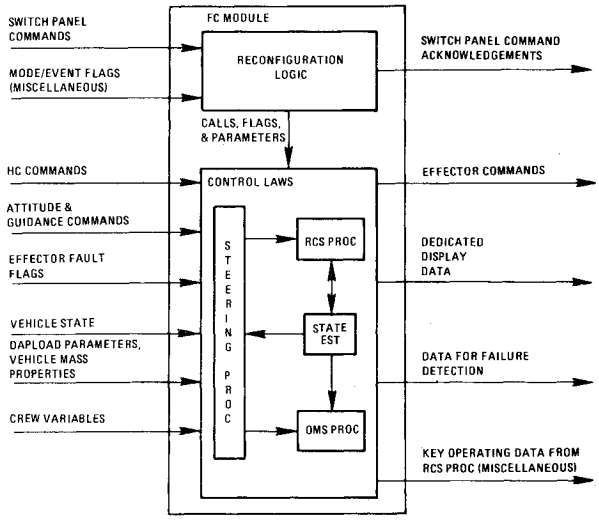

Fig 2 Flight control module configuration.

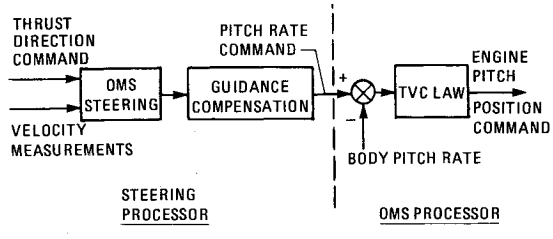

Fig. 3 Block diagram of steering and OMS processors for pitch channel.

The steady-state gain determines the bandwidth and the speed of response of the loop. The main function of the filter is to attenuate the high bending frequencies and filter the quantized commands and rate gyro quantization effects and noise The purpose of the integral compensation is to minimize the effects of thrust misalignment relative to the vehicle center of gravity while also eliminating any steady-state rate error. Without the integral compensation, the steady-state error is nonzero and its magnitude depends on the dc gain of the TVC law. Additionally, the integral compensation makes the forward loop gain infinite, thus eliminating any steady-state rate error that might result from a constant bias in the thrust position relative to the engine servo command.

The digital output of the TVC law goes to a zero-order hold to obtain the engine gimbal servo position command as a continuous signal.

The open-loop frequency response of the compensated system is shown in Fig. 5 in gain vs phase plots for three amplitudes of signal level applied to the actuator hysteresis nonlinearity. The actuator was approximated by first-order lags at 6.3, 3.5, and 1.9 rad/s for signal levels of two, four, and eight times larger than the hysteresis.

The plots were generated by incrementing the fictitious w-plane frequency, and the real frequency marks indicated on the plot were obtained by the transformation $\omega = 2/T \tan^{-1} w$, where T is the sampling period of 0.08 s. The crossover frequency is 0.8 rad/s with a phase margin of 65 deg and gain margin of 18 dB. The phase margin diminishes for increasing signal amplitudes to 60 and 50 deg, while the gain margin remains unchanged. Propellant slosh, occurring at 1.55 rad/s, is phase stabilized since the loop in the plot caused by slosh moves away from the critical 0 dB, -180 deg point. The bending modes are gain stabilized with 42 dB attenuation in the first mode. Although this theoretically derived bending margin is quite substantial, it must be pointed out that data uncertainties can rapidly decrease the actual margin in two ways: first if the frequency of the mode is lower than predicted, and, second, if the amplitude of the loop caused by bending is larger. When coupled with a rigid body, the bending resonances create nearby antiresonances in the transfer function and both appear in the gain vs phase plot as loops, superimposed on the rigid-body plot, similar to the one shown in Fig. 5. The amplitude of the loop depends on the pole-zero separation (i.e., on the bending data) and the damping ratio (here $\zeta = 0.005$ was assumed). Allowing for a frequency uncertainty of 30% and an additional increase in the resonance peak of 10 dB, the gain margin diminishes to 15 dB, which is still satisfactory.

Outer Loop

As shown in Fig. 6, the outer-loop block diagram, which has a processing rate of 1.04 Hz, includes the OMS steering module and the velocity measurements. The OMS steering

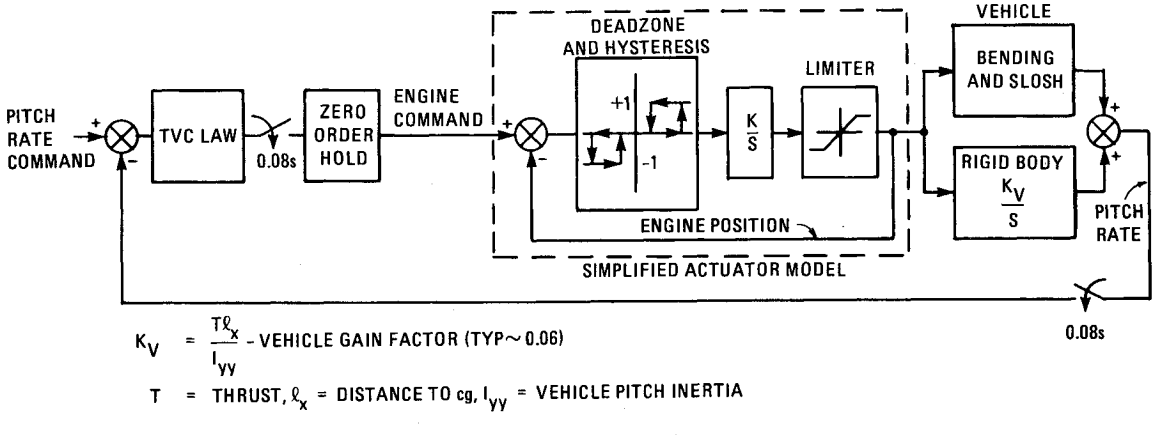

Fig. 4 OMS TVC inner loop for pitch channel.

module generates an angular rate command proportional to the cross product of the commanded thrust direction, $\bar{V}_{go}$ and the sensed velocity change, $\bar{V}$. The commands for OMS steering go to the guidance compensation module and then to the inner loop. As mentioned before, these modules are processed at the higher sampling rate of 12.5 Hz and, therefore, in order to facilitate the analysis of the outer loop, they are approximated by continuous transfer functions.

The guidance compensation output is the rate command for the inner loop. This module provides gain, compensation filtering, and limiting for the outer loop. The purpose of the lag-lead filter is to maintain the stability of the loop at a higher gain level than would have been possible by simple gain compensation. The higher gain results in lower peak cross-axis velocity errors and better performance in short burns.

It can be shown[2] that the quantity $(\theta-\delta)$ followed by an integrator yields appropriate velocity increments for the cross-product steering computation performed by orbital maneuvering system steering. The transfer function from the rate command input ω_c to $(\theta-\delta)$ is

$$\frac{\theta-\delta}{\omega_c}=\frac{\omega}{\omega_c}\frac{1}{s}\left(1-\frac{K_v}{s^2}\right)$$

where ω/ω_c is the closed-loop transfer function of the inner loop, and the $(1-K_v/s^2)$ factor is a pair of zeros. The vehicle gain, K_v, is typically 0.06 and the zero values resulting from it occur near the loop crossover and interfere with the needed rolloff in magnitude. The guidance compensation filtering provides some of this needed attenuation.

The gain vs phase plot of this loop made in the w-transform plane is shown in Fig. 7 with appropriate transformations to real frequency indicated in the plot. The crossover frequency is 0.087 rad/s and the phase margin is 70 deg for the case of time to the end of the burn, T_{go}, which is very large. However, as T_{go} diminishes the phase margin decreases. As shown in the figure, the phase margin is only 22 deg at $T_{go}=10$ s. Therefore, the outer loop is disabled 6 s before the end of the burn.

In addition to the analytical approaches described above, the design process uses an engineering computer simulation to verify the transient response of the design and to finalize certain nonlinear elements or parameters such as command and integrator limiters and phase-plane upper and lower rate limits and deadbands.

Performance Evaluation

The performance of the OMS TVC system was tested before flight on several high-fidelity simulators that included flight hardware and computers, and in flight on three Shuttle test flights. However, the engineering simulation developed for the evaluation proved to be invaluable because of its simplicity and cost effectiveness.

This six degree-of-freedom simulation included a rigid-body vehicle; the nonlinear actuators represented by simplified models (described previously); fast and slow sampling rates for the inner and outer loops; rate gyro quantization, noise, bias, and the bias correction scheme; inertial measurement units (IMU) mounted (ahead of the center of gravity) accelerometers; accelerometer quantization; provision for reading in various vehicle mass properties; phase plane, the RCS jet-select logic; and numerous other options for considering off-nominal situations such as engine failure, actuators failing in a variety of ways, and RCS jet-on and jet-off failures. Initially, this program did not include slosh and bending dynamics, but a simple bending model was incorporated to study RCS/bending interaction and to test a digital rate gyro filter that was developed to alleviate this problem.

As shown in the design section, the slosh dynamics were phase stabilized by the controller design. In addition, an analytical derivation of possible OMS propellant slosh effect has shown that its effect would be so small that the worst case (i.e., all slosh masses in the OMS tanks acting in unison, starting with the maximum possible initial slosh displacement) would result in body rates that would not exceed the rate gyro quantization levels. For this reason, the slosh model was not incorporated in this simulation or in any verification work.

Nominal Performance

An example of OMS TVC performance in a 100 ft/s burn is shown in Fig. 8. The only initial error assumed was a 5 deg attitude error. As indicated, the initial cross-axis velocity error buildup is sensed by the steering resulting in a pitch rate command. The pitch rate response follows closely with the effect of initially checking the buildup of the velocity error and subsequently turning it around and reducing it to near zero at the end of the burn. The only significant gimbal deflections occur at the beginning, and for the rest of the burn the gimbals respond mainly to quantization effects and rate gyro noise.

The effect of thrust misalignment of nominal magnitudes up to 1 deg results in a similar response for two reasons: 1) the thrust misalignments are rapidly taken out by the inner loop; and 2) due to the very low gain of the vehicle, the attitude buildup resulting from the misalignment is very small and the burn performance is a scaled-down version (as far as errors are conerned) of Fig. 8.

Failure Cases

Off-nominal burns were studied extensively with particular attention paid to RCS fuel penalties resulting from activation of the RCS assist mode of operation. Performance results for a 200 ft/s burn are given in Table 3, and the description of the

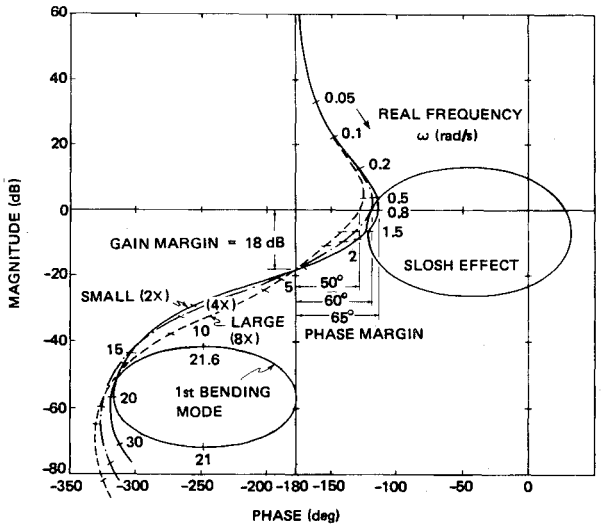

Fig. 5 Magnitude vs phase of OMS TVC pitch inner loop for three signal levels applied to actuator nonlinearity.

Table 3 RCS fuel expenditures and velocity errors for the failure cases

Case	RCS fuel, lb	Peak velocity errors, ft/s V_z	Peak velocity errors, ft/s V_y	Cutoff velocity errors, ft/s
1	24	1.0	5.7	<0.1
2	34	1.1	4.0	<0.1
3	32	1.1	4.0	<0.1
4	187	10.3	2.2	<0.1
5	179	8.9	6.8	<0.1
6	526	9.7	6.8	4.9
7	321	7.1	4.4	3.9

cases studied is given below (all cases include an initial 5 deg attitude error in both pitch and yaw):

1) A one-engine burn starting with two-engine gimbal trims. This represents the hypothetical case of a single-engine burn initiated without the crew's ability to change the initial trim (set to two-engine values) but with a knowledge that it will be a one-engine burn and with the system reconfigured for this condition.

2) One engine failed at 0 s, no reconfiguration.

3) One engine failed at 0 s, reconfiguration at 30 s into the burn.

4) A pitch actuator failed hardover at 0 s, the standby actuator switched in at 40 s.

5) The pitch and yaw actuators failed hardover at 0 s and the standbys switched in at 40 s.

6) The pitch and yaw actuators failed hardover at 0 s and the standbys not switched in.

7) A large torque disturbance from two RCS jets failed on at 40 s and removed at 60 s (RCS fuel expended by the failed jets is not included in the table).

The failure cases listed fall into two categories: OMS related (engine or actuator) or a failure external to OMS such as the RCS jets failed on. OMS failure by slight thrust degradation is readily compensated for by the other engine. In the event of the total failure of one engine, the resultant RCS fuel usage for the burn, as shown in Table 3 for the first three cases, is relatively small and is expended for roll control by the RCS. The velocity errors got to values as high as 5.7 ft/s, and, if the failure occurred at the most disadvantageous time during the burn, the cutoff velocity error could assume nearly this value.

The actuator failures (only hardover failures are shown) are costlier in both RCS fuel consumption and velocity errors. Of the two actuators, the pitch hardover failure case is worse. If the yaw actuator goes hardover, the other engine will balance it to the extent possible; i.e., it will go as far as the software limit, which is 1.56 deg smaller than the hardstop limit, leaving this unbalance as a torque disturbance. However, in a pitch hardover case the other engine will go to its software stop in order to take out the pitch disturbance, leaving not only a pitch torque unbalance but also creating a large roll torque disturbance.

Comparing case 4 with pitch only and case 5 with pitch and yaw actuators both hardover, it is seen that the RCS fuel penalty is essentially the same and the velocity error peaks, although slightly different, have RMS values that are about the same.

If the hardover situation stays uncorrected throughout the burn, as shown for case 6, the RCS fuel consumed is 526 lb and the cutoff velocity error is 4.9 ft/s.

The case of two RCS jets failed on for 20 s during a burn is also very costly. With OMS control authority significantly less than the RCS authority, the torque disturbance causes an almost continuous RCS counterfiring. The disturbance to the system is so severe that in the remaining burn time the velocity error is reduced to only 4 ft/s.

Flight Experience

No severe failures of the types simulated were encountered during the first three Shuttle test flights. All of the burns were nominal, terminating with velocity errors significantly smaller than 1 ft/s.

In addition to the listed hardover actutor failures, two other types of actuator failures were studied. These were cases of stuck actuators and actuators with open feedback loops. The results were found to be more benign than hardover failures. Ironically, during STS-1, a type of actuator failure occurred that was not anticipated and considered. During gimbal drive tests, the astronauts noticed that one of the pitch actuators did not initially drive in the negative direction and subsequently drove sluggishly, i.e., at an easily detectable reduced rate,

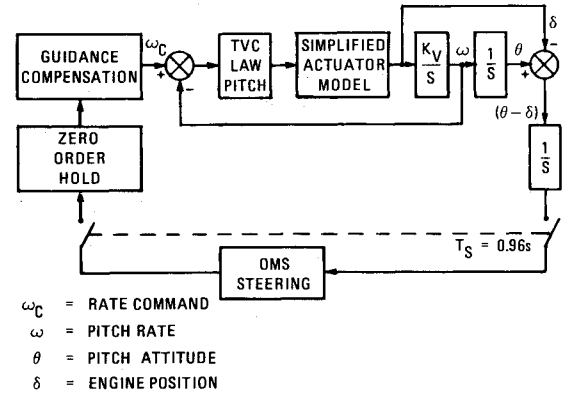

Fig. 6 OMS TVC outer/guidance loop block diagram.

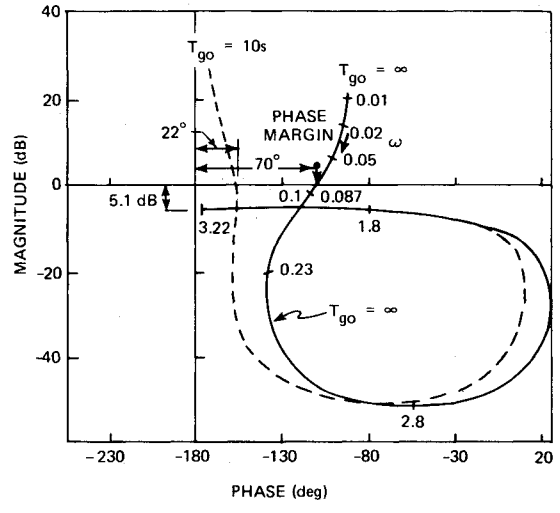

Fig. 7 OMS TVC pitch outer-loop magnitude phase.

while the performance of drive in the positive direction was nominal. Since there was still a crucial deorbit burn to be performed, a study was performed quickly on the engineering simulator and the results showed that for a number of reduced rates from the nominal value of 4 to 1 deg/s, the performance degradation was insignificant. Even at the minimal rate of −0.1 deg/s, the performance was still acceptable with only a slight RCS fuel penalty of 17 lb in the deorbit burn. This information was passed on to Mission Control, and the burn was performed successfully using standby actuators but with the crew instructed not to hesitate to switch to the sluggish primary actuator in the case of actuator failure.

The only anticipated nonfailure type of disturbance occurred during the OMS-1 burns. It was produced by the planned dump of residual main propulsion system propellant trapped in the feed lines. Prior to STS-1, many simulations were run to evaluate these effects. The oxygen dump, done through the main engine, was beneficial in reducing required OMS propellant to achieve the desired velocity change. The hydrogen dump, done through a port side valve, was found to produce orbiter angular rate transients well within the TVC control authority. Simulation showed significant rate needle transients at dump initiation that could create some crew confusion in the event of a manual takeover during OMS failures, but no control recovery problems existed in the automatic TVC mode. Space Transportation System (STS) flight data confirmed the results, though the roll disturbance rate profile was more pronounced than in the simulation. The reason was shown to be hydrogen plume impingement on the wing, which was not modeled before flight but which conformed with theoretical models.

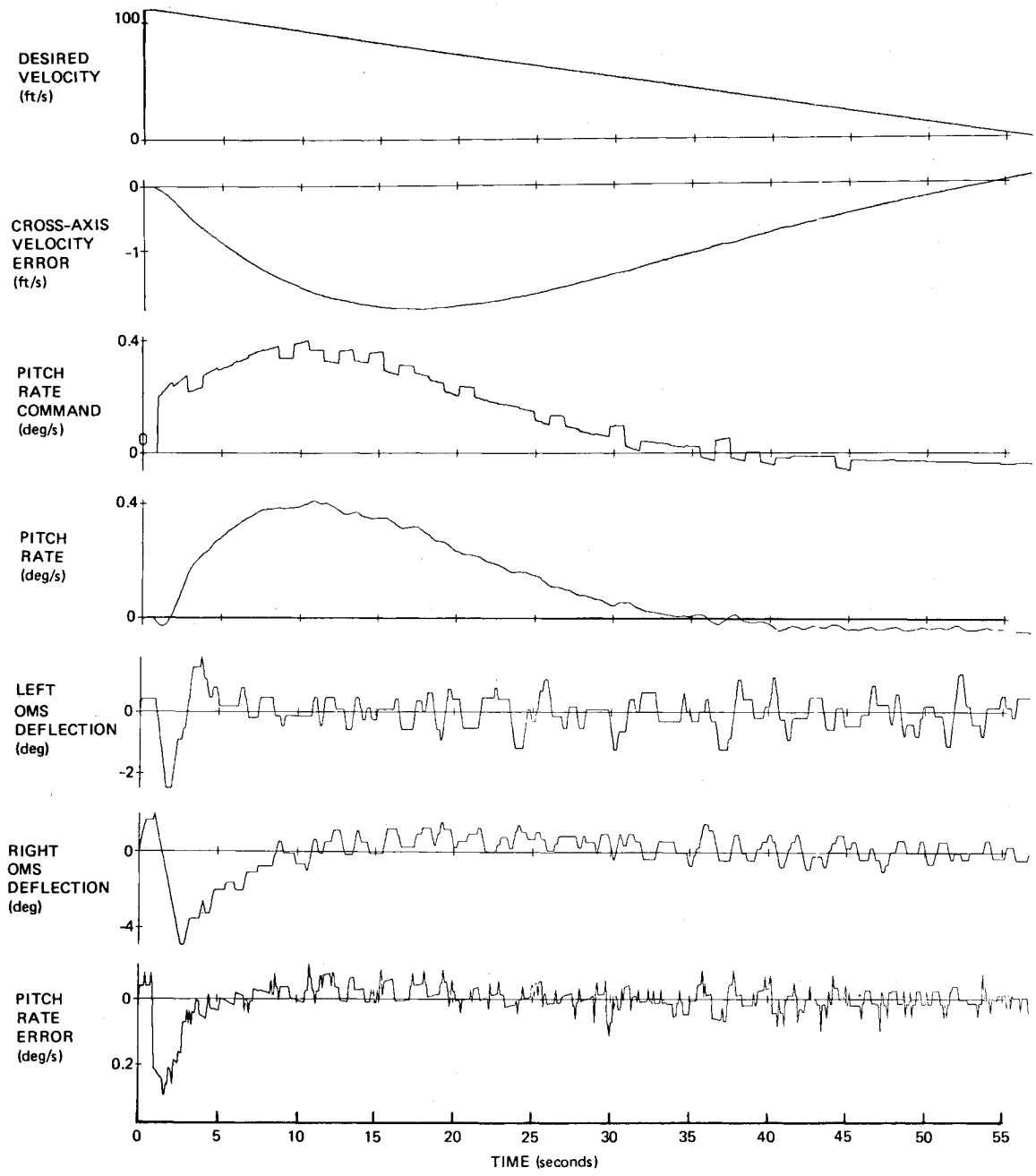

Fig. 8 Typical OMS TVC pitch performance in a 100 ft/s burn.

Conclusion

The orbital maneuvering system thrust vector control described in this paper flew on the first three Shuttle test flights. The fourth Shuttle mission, which concluded the series of test flights, used the same orbital maneuvering system thrust vector control design. For operational flights, the design has been modified slightly but the design methodology is the same as described herein.

An assessment of the orbital maneuvering system thrust vector control flight performance would not be complete without the commentary made by astronaut Crippen, pilot of STS-1, at the crew debriefing: "Everything with regard to the OMS burn was smooth. Every time we used the OMS, it was beautiful."

Acknowledgment

The material presented in this paper is the result of a multiyear collaborative effort which included flight control/autopilot expert staff at The Charles Stark Draper Laboratory, Inc., NASA, Rockwell International, Lockheed, and Honeywell. The authors would like to express special appreciation to Philip Hattis and Christopher Kirchwey of CSDL and to Edward T. Kubiak and Kenneth L. Lindsay of the NASA Johnson Space Center, who managed the transition and on-orbit autopilot designs respectively, for their contributions to this effort.

This paper was prepared by The Charles Stark Draper Laboratory, Inc., under Contract NAS9-16023 with the National Aeronautics and Space Administration. The work was supported by NASA Johnson Space Center.

Publication of this report does not constitute approval by NASA of findings or conclusions contained herein. It is published for the exchange and stimulation of ideas.

References

[1] "Orbial Maneuvering System Actuator Test," NASA JSC Internal Note 78-EG-3, March 1978.

[2] "On-Orbit Flight Control Algorithm Description," Charles Stark Draper Laboratory, Rept. R-881, Jan. 1976.